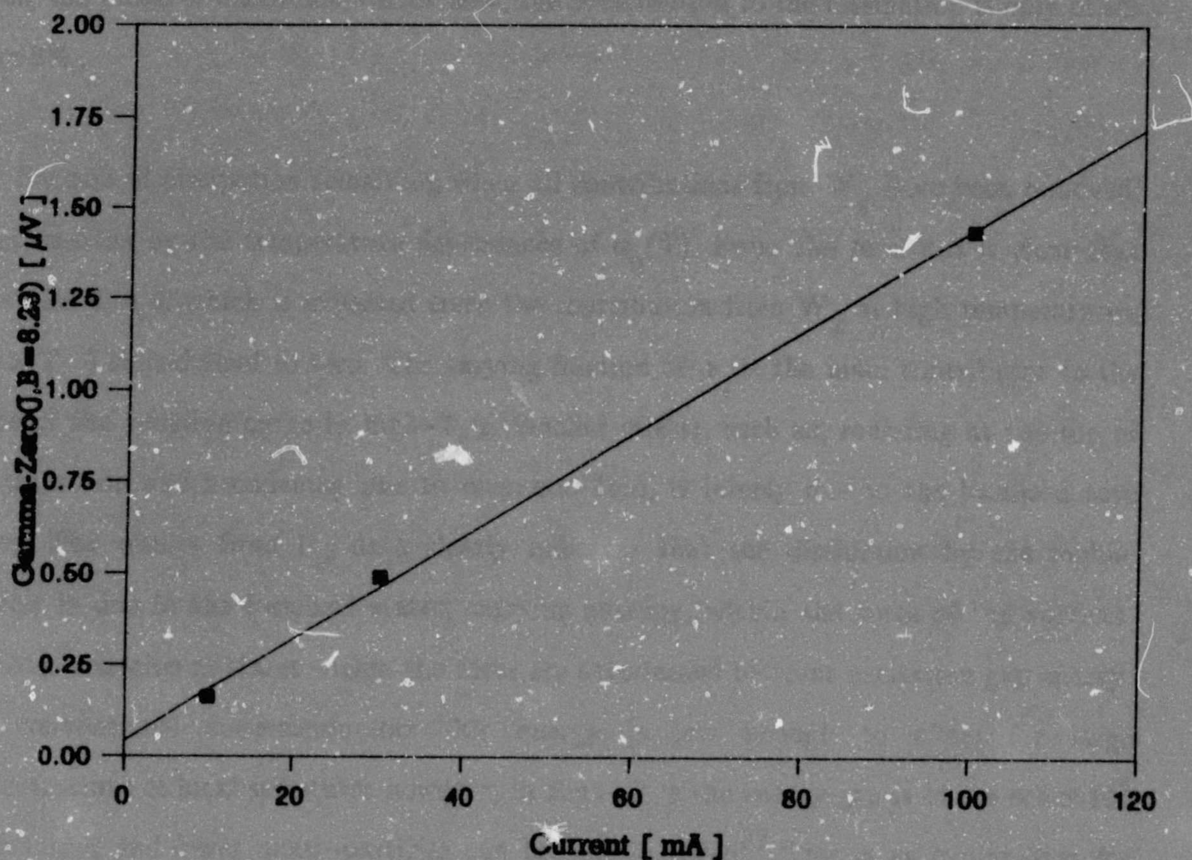

Figure 3.10 A plot of $\Gamma_o(J,B = 8.29\ T)$ versus I. The direct proportionality implies the dependence of the effective rate of vortex rotation, ν_{eff}, on the current.

The most striking result from the analysis of Γ_φ is the absolute values of the peaks, where the maximum dissipation due to vortex motion occurs. Comparing the peak values to the corresponding voltage values at the same temperature for the W(T) curves, indicate that during the phase of maximum vortex flow, the contribution to the dissipation is only of the order 2% .

The fraction of dissipation remaining when all contributions from W_φ have been removed, is represented by the temperature dependence of $\alpha_q(T)$. From the results it is clear that $\alpha_q \to 1$ as $T \to \infty$, which is expected since the contribution from W_φ at high temperatures, ($T > T_c$) should tend to zero. The varying fraction of α_q is the main contributor to the shape of the resistive curve in high–T_c's. Smaller effects, such as, rounding at the top of the transition and broadening due to magnetic field, is largely due to the localised core states. The results from Γ_φ data clearly indicates that the dissipation by the mobile vortices is due to the localized states, carrying entropy, within the cores of the vortices. The concentration of states within the cores are determined by some excitation gap energy. For conventional superconductors this energy is low enough to allow for large concentrations of localised states however, in High–T_c's the energy gap is of the order 10^4 times larger and fewer quasi–particles can become localised.[37] This is an explanation for the very small dissipative contribution to the total resistivity from the mobile vortices. Alternatively, dissipation in conventional superconductors can be ascribed mainly to the motion of vortices carrying entropy through their localised core states. However, this is not the case for the new High–T_c materials where this particular study has verified that dissipation occurs largely through the normal scattering processes of quasi–particle extended states.

3.3 Results and Discussion for the Effective Activation Energy U_o

The rise in the curve for Γ_φ below $T_c(B)$ resembles an exponential form and hence the altered expression for TAFF (equation 3.8), is well suited to this region. The measurements were conducted at discrete temperature intervals to ensure good thermal stability. This, however, did not allow for an excellent point density in the region of interest. For all of the LSQ fits considered below, no fewer than 6 points were considered in the temperature interval used for the fit. The use of 6 points made the fit statistically reasonable as well as, ensuring that the theoretical curve had the correct shape to incorporate the low temperature data within the noise and the data just below $T_c(B)$. Theoretical fits to 2 fields are represented in figure 3.11 for the same current. Table 3.2 displays the full set of results for all twelve data configurations, also including the temperature independent term, $\Gamma_o(J,B)$. The results for the activation energies are consistent with regard to the current and expected field dependence. The larger the Lorentz force, $J \times B$, becomes; the average pinning force is subsequently reduced and hence the activation energy required to overcome these forces is also reduced. The $\Gamma_o(J,B)$ term increases with increasing current and magnetic field, and implicitly ν_{eff}, is expected to increase accordingly.

The values for U(B), as listed in Table 3.2 show a definite current dependence, and therefore an alternative form to this activation energy is suggested, (see APPENDIX A):

$$U(J,B) = U_o \cdot \mathrm{Log}[J_c/J] \cdot \exp[-B/B_o] \qquad 3.10$$

For each field the three current dependencies are removed firstly, by plotting U(J,B) as a function of Log[J], and obtaining $U(B) = U_o \cdot \exp[-B/B_o]$ from the slope of the straight line, (figure 3.11a below). Secondly, U_o, the effective pinning energy is found by plotting Log[U(B)] versus B for the four fields, (figure 3.11b). The excellent linear regression

Table 3.2

Below, the full set of results are tabulated for the activation energy, U(I,B), in K, [Light print]; and the current dependent, $\Gamma_o(I,B)$, in μV, [*Italics*].

	10 mA	**30 mA**	**100 mA**
0.89 T	6741.5 *1.00e-7*	3671.3 *1.94e-7*	3009.3 *8.04e-7*
1.78 T	5196.7 *1.01e-7*	3154.5 *2.68e-7*	2488.6 *9.91e-7*
3.55 T	3956.1 *1.28e-7*	2642.1 *2.95e-7*	2162.4 *9.77e-7*
8.29 T	2256.3 *1.61e-7*	1868.4 *4.89e-7*	1652.0 *14.35e-7*

results that are obtained for both current and field dependencies, show that the alternative form of the activation energy, U, is a very good approximation to the data of this experiment. From the data the effective activation energy is found from the intercept of the straight line, $U_o = 0.15 \pm 0.01$ eV. It is interesting to note that this value found for U_o is comparable to a value found by Sengupta et al,[74] in YBCO single crystals, at which a discontinuity occurs in their U–J curve. This discontinuity corresponds to the flux–pinning energy. (the inherent potential energy wells), for current densities below a corresponding value for J, U rises sharply, as no activation can occur. Also a value for the Proximity breakdown field, was found to be $B_o = 4.28 \pm 0.08$ T. The inset of figure 3.11b shows an interesting, alternative power–law behaviour of U(B) with the current dependence removed, i.e. $U(B) = A \cdot B^n$, where $A = 0.12 \pm 0.1$ eV, and $n = 0.67 \pm 0.02$, ($n \simeq 2/3$).

According to deGennes[27], the breakdown field is of the form,

$$B_o = [\hbar/v_F]/[\sqrt{12}\, e \cdot D_N \cdot d_N] \qquad 3.11$$

which allows the size of the intrinsic normal region, d_N, to be estimated. With $D_N = \ell v_F/3$, the result, $B_o = 4.28$ T, and taking an accepted average value for the mean free path, $\ell \simeq 150$ Å, ($100 \text{ Å} \leq \ell \leq 200$ Å)[75] at T_c, equation 3.11 gives $d_N \cong 90$ Å.

From APPENDIX A, the effective pinning potential, U_o is related to the correlation length along a flux line, L_c, as

$$U_o = J_c(0)\varphi_o L_c \zeta_o \qquad 3.12$$

and taking typical values of $J_c(0) = 10^8$ A/m², $\zeta_o = 15$ Å with the result found for $U_o = 0.15$ eV; we have that, $L_c \simeq 85\ \mu$m.

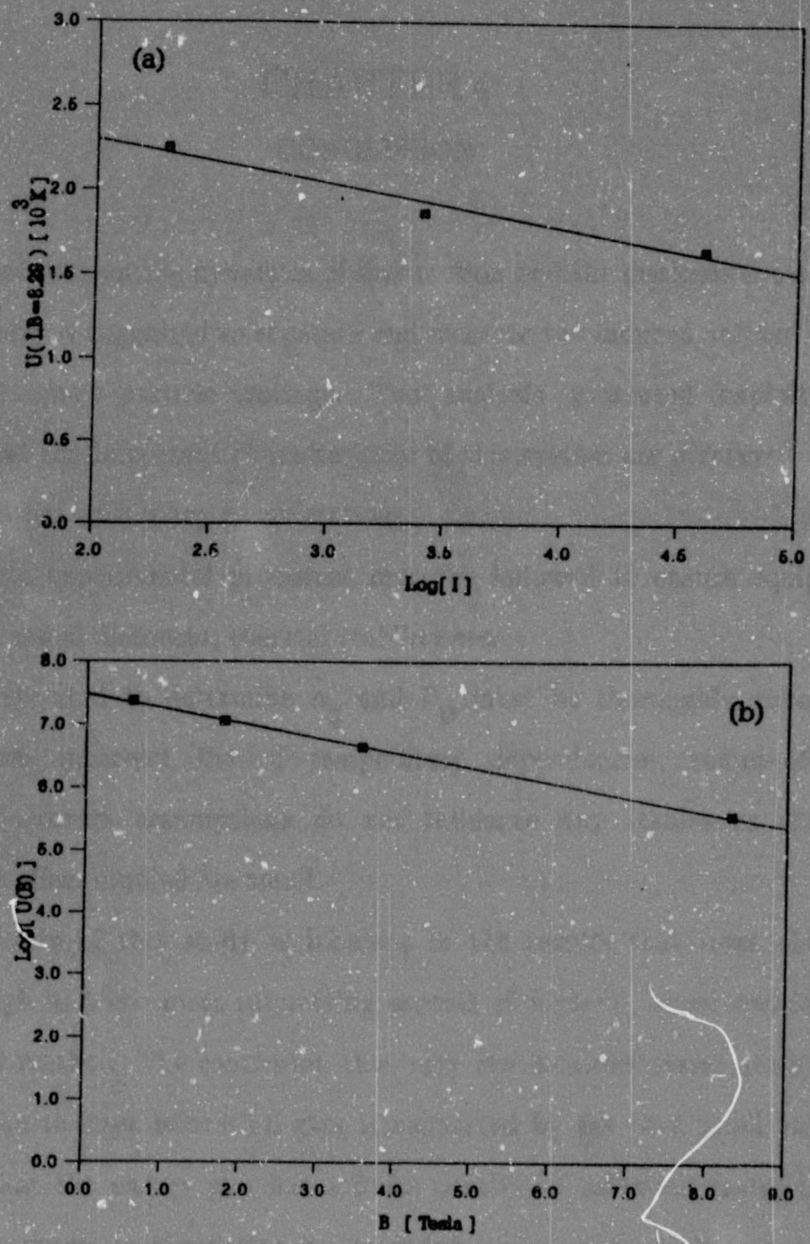

Figure 3.11 (a) A plot of U(I,B) versus Log[I], to remove the current dependence from the activation energy. Straight line fits to the data provided good results with, 0.93 < r 0.98, indicating validity of Log[J_c/J] term. (b) A plot of Log[U(B)] as a function of B. The current independent data provided an excellent fit (r = 0.999) for the four field values.

CHAPTER 4

CONCLUSION

This study concentrates on the dynamics of flux motion and the dissipation associated with it. A novel geometry is suggested to separate and measure the induced voltage contribution and the normal quasi--particle voltage. The analysis presented exploits the data successfully so that the important characteristics of this system are displayed. The success of this experiment lies with many considerations:

i) An accurate experimental procedure must be followed to ensure equipotentiality, correct values for radial distances, thermal stability etc.

ii) The analysis used to determine α_q and Γ_φ must be thoroughly checked so that contributions from incorrect fits of temperature dependencies, round--off errors in computing and incorrect assumptions do not influence any results as the orders of magnitude for the effect studied are small.

However, the success of this study is inherent in the results that were obtained. The method is thorough and the most interesting aspects of high--T_c superconductors can be studied using this method. The conclusion that very few localised states are bound within the vortex core due to large excitation gaps is supported by the very small values for Γ_φ. The suggestion that the energy gap has a finite density of extended states may also be supported by this study as dissipation by extended states occurs well below the critical transition temperature. In conventional superconductors the dissipative process is governed by the motion of vortices through the various stages of flux motion until after T_c, the quasi--particle – phonon scattering processes lead to the usual metallic behaviour of the materials. This study has shown, for YBCO in particular, that the maximum contribution from localised core states occurs well below T_c and only contributes a very small fraction to the dissipation. Hence, it is concluded that for high--T_c materials, extended quasi –

particle excitations are the characteristic contributors to the dissipation, for temperatures well below the critical transition temperature.

In APPENDIX A, an alternative form of the activation energy is suggested to account for the current dependence displayed by the activation energy. The fact that the data fits very well to the assumed function, substantiates the author's reasoning for including the $Log[J_c/J]$ current dependence. It must however be noted that the true current dependence cannot accurately be determined with only three distinct densities; and hence this finding calls for an in–depth investigation of the current dependence U(J) for the regime, $J << J_c$

The confirmation that vortex propelled by a Lorentz force in a disc shaped sample, leads to circular motion provides further interesting studies. The exchange of entropy that accompanies flux flow across boundaries can be utilised to study thermoelectric effects. By applying a thermal gradient with a Lorentz force, the dynamics of the vortex motion within a circular geometry can amplify thermoelectric effects that are too small to be measured using traditional techniques (e.g. Ettinghausen).

APPENDIX A

INTRINSIC SUPERCONDUCTOR–NORMAL PROXIMITY EFFECT AND ITS INFLUENCE ON THE THERMALLY ACTIVATED FLUX FLOW MODEL

This appendix is included as an aside to the main study, however, the very interesting characteristics displayed by the sample, justify an explanation and derivation of the results. The author is grateful to Drs Gridin and Sergeenkov for the inclusion of the results prior to publication.[66]

Hsiang and Finnemore[67] demonstrated a suppression of the critical current, J_c, for a superconductor – normal metal – superconductor junction, (SNS), in a magnetic field. They found that J_c decreases exponentially with increasing magnetic field H; and the decay length of the order parameter, decreased linearly with applied field as expected. A similar study was conducted on $YBa_2Cu_3O_{7-\delta}$ thin films[68] and the exponential dependence on the magnetic field was ascribed to intrinsic SNS junctions formed by the crystallographic defects. On the application of a sufficiently large current density, these weak links go normal or alternatively, act as a point most susceptible to thermally activated flux flow. Bougrine et al[69] have also applied the above approach to their anomalous thermal conductivity data. The field dependence of the bound vortex – phonon scattering was described using the behaviour of the 'proximity induced critical current', (see below).

APPENDIX A

The specific sample geometry used in this study provided a suitable mechanism for the intrinsic proximity effect to occur. By the very design of the current input into the sample, the centre of the disk was driven 'normal' sooner, as the current density decayed as 1/R towards to rim of the disk. This expanding current density provided sites within the sample that were driven normal and formed weak links with superconducting regions. These sites either act as pair breaking mechanisms for the already rotating vortices or as suitable centres for the thermally activated flux flow of vortices.

Below follows a derivation for the intrinsic proximity mediated activation energy discussed in section 1.2.4.3, and especially for equations 1.2.8 and 1.2.9.

The induced voltage contribution, Γ_φ, from the rotating vortices can be interpreted by means of the TAFF model, as the current densities used are in the low current density limit as described by Kes and van den Berg[51], ($J << J_c$). Γ_φ is assumed to be of the form,

$$\Gamma_\varphi(J,T,B) = \Gamma_0(J,B)\cdot\exp[-U(T,B)] \qquad \text{A.1}$$

where U(T,B) is an effective reduced activation energy mediated by the intrinsic proximity effect. In the absence of a driving force the pinning potential, (effective activation energy), can be related to the critical current density by[48,49],

$$U(T,B) = J_c(T,B)\cdot B\cdot V\cdot a \qquad \text{A.2}$$

where V is the volume of flux lattice within the range, a, of the pinning potential, (see equation 1.2.3). For most High–T_c's the inherent vortices have little or no long–range order; they are randomly arranged in spatially amorphous manner; which is due to the randomness of the pinning itself. In these materials, vortex pinning sites possibly include oxygen vacancy–type positions and other atomic disorder that may arise from slight deviations in the stoichiometry, twin boundaries, etc. (see section 1.2.4.2). In this region of magnetic fields where the distortion of the flux line lattice occurs, the flux volume, V, can be approximated by,

$$V \cong L_c \cdot a_o^2 \cong L_c \cdot (\varphi_o/B)^{1/2} \qquad \text{A.3}$$

using Abrikosov's flux lattice parameter, $a_o(B) \simeq (\varphi_o/B)^{1/2}$. L_c is the correlation length along the flux line, or the longitudinal size of the region in which there is a short–range order.[70] For the case of $B < 0.2\ B_{c2}$, considerable differences may occur between the hopping distance w, and the range of the pinning potential, a. For this particular study, the magnetic fields used fall within this range and hence, w is of order a_o and $a \simeq \xi(T)$.[48]

In the low field regime, the behavior of the proximity induced critical current obeys the relation[27],

$$J_c(T,B) = J_c(T) \cdot \exp[-B/B_o] \qquad \text{A.4}$$

with, $1/B_o = (2\sqrt{3}\ d_N D_N e)/(\hbar \cdot v_F)$, and

APPENDIX A

$$J_c(T) = J_c(0)(1-t)^2, \text{ where } t \equiv T/T_c(B) \qquad \text{A.5}$$

here D_N, v_F and d_N are the diffusion length, Fermi velocity and the thickness of the normal junction, respectively.

Substituting equations A.3 – A.5 into equation A.2, and using the result, $\xi(T) = \xi_o \cdot (1-t^2)^{-1/2}$, the pinning potential or effective activation energy due to the intrinsic proximity effect is,

$$U(T,B) = J_c(0)\varphi_o L_c \xi_o \cdot (1-t^2)^{3/2} \exp(-B/B_o) \qquad \text{A.6}$$

$$= U_o \cdot \exp(-B/B_o) \cdot (1-t^2)^{3/2}$$

$$= U(B) \cdot (1-t^2)^{3/2} \qquad \text{A.7}$$

Returning to the prefactor of equation A.1, $\Gamma_o(J,B)$, where it is important to define if experimental results are compared with the TAFF expressions. From Kes et al[48] Γ_o for the proximity mediated effect is assumed to have the form,

$$\Gamma_o(J,B) = U(T,B)/\beta_c \cdot [J/J_c(T)] \cdot [K \cdot w/a] \qquad \text{A.8}$$

where, $\beta_c = 1/k_B T_c$, $K = \hbar B/m_e S$, ($S = \pi R^2$). Substituting for U(T,B) and using equation A.5 with the approximations for w and a, it can be shown that Γ_0 is proportional to,

$$\Gamma_0(J,B) \;\alpha\; J \cdot B^{1/2} \exp[-B/B_0] \qquad \text{A.9}$$

From the data for Γ_φ fits to the above expression (A.1) can be performed to find U(B) and Γ_0(J,B). In view of equation A.1 the activation energy is found from the exponential term, and not from Γ_0(J,B). In the above analysis, the activation energy resulting from this type of fit to the data, is independent of current. For the low current density regime, ($J << J_c$), it is theoretically predicted that U should grow with decreasing current[71,72]. It has been experimentally observed that $U(J) \simeq U_0 \cdot Log[J_c/J]$ is a good approximation for single vortex creep in the 3D case.[73] With this approach it seems reasonable to propose an alternative form of the activation energy resulting from the exponential term of A.1:

$$U(T,J,B) = U_0 \cdot Log[J_c/J] \cdot \exp[-B/B_0] \cdot (1-t^2)^{3/2} \qquad \text{A.10}$$

with, $U(B) = U_0 \cdot \exp[-B/B_0]$, the current and field dependent form is,

$$U(J,B) = U(B) \cdot Log[J_c/J] \qquad \text{A.11}$$

Hence, the current dependence of the activation energy can be removed from U(J,B) by plotting, U(J,B) as a function of Log[J], and finding U(B) from the slope of the resulting straight line. The effective pinning activation scale, U_0, (Current/field independent) can now be estimated, by plotting Log[U(B)] versus B for the different fields, and finding U_0